Controlling of Variable Structure Power Electronics for Self-Contained Photovoltaic Power Technologies

Ashutosh Kumar Singh[1] and Chirag Gupta[2]

[1] Department of Electrical & Electronics Engineering,Vedica Institute of Technology, RKDF University, Bhopal, India
[2]Department of Electrical & Electronics Engineering,Vedica Institute of Technology, RKDF University, Bhopal, India
[1]ak.singhbgp95@gmail.com, [2]cgupta.011@gmail.com

* Corresponding Author: Ashutosh Kumar Singh

Abstract: *For photovoltaic energy conversion systems, a self-contained-control-based power conversion technique is developed. For maximising the power generation capacities from solar panels, the perturbation and observation (P&O) maximum power-point tracking (MPPT) technique is used. We must use a nonlinear control technique to maximise the energy conversion efficiency and to withstand fluctuations and variations in load and sunshine irradiance due to the inherent nonlinear dynamics of power converters. Novel first- and higher-order sliding mode control approaches are proposed in this paper, with the goal of developing a systematic approach for the robust and optimal control of solar energy conversion that ensures Lyapunov stability and consistent performance in the face of external perturbations and disturbances. Furthermore, super-twisting second-order sliding mode control for the buck-boost converter is created to minimise the chattering phenomena inherent in the first-order technique. In addition, the output of the DC–DC converter feeds a space-vector pulse-width-modulated inverter with voltage-oriented control (VOC) to provide three-phase AC power for the grid. Computer simulations and the dSPACE hardware-in-the-loop platform have been used to examine the proposed sliding-mode-control-based solar energy conversion system to verify its resilience and efficacy.*

Keywords: *sliding mode control; DC–DC converter; solar energy systems*

I. Introduction

One of the most promising renewable energy resources of the twenty-first century is solar power generation, particularly photovoltaic (PV) electricity. Photovoltaic panels exhibit variable output characteristics under changing weather, load fluctuations, and shifting sunlight irradiation circumstances due to the semiconductor material features of solar cells. The key to increasing power output and lowering power losses is dynamically matching the internal resistance of solar panels with the corresponding Thevenin resistance of the power system [1]. As a result, maximal power-point tracking is critical for energy conversion efficiency optimization. The time-varying DC-link voltage at the output of DC–DC converters is one of the primary control issues of a PV system. To reduce output voltage changes and ensure a steady DC voltage level, flexible distributed power production with significant penetration in PV panels necessitates a robust DC–DC converter management strategy. Despite the nonlinear nature of DC–DC converter characteristics [2], classical PID control based on Jacobian linearization of nonlinear dynamics is the most commonly used control approach in practical high-power converter applications, which typically provides poor performance and low power conversion efficiencies. To obtain superior performance under high-level system nonlinearity, time-varying solar irradiation, and load variations settings, a resilient and effective nonlinear control approach is desired [3–5]. The slidingmode control approach has been one of the most extensively utilised nonlinear control strategies for powering electronic devices among many nonlinear control methods [6].

The perturbation and observation (P&O) MPPT method is used to operate a commercially available 270W "SolarWorld Sunmodule-Plus SW 270 Mono Black" solar panel to achieve maximum power-point tracking (MPPT). For the buck-boost converter, unique first- and higher-order sliding mode control techniques are designed to maximise power conversion performance. The whole photovoltaic energy conversion system is depicted in Figure 1. The PV module's output is channelled into the boost converter, which allows for maximum power point tracking (MPPT). The MPPT controller receives the measured solar panel voltage V_{panel} and current I_{panel}, and the MPPT controller's output adjusts the boost converter's output to match the voltage needed for charging the battery pack. The battery is then fed through the buck-boost converter, whose output is coupled to the common DC connection. The buck-boost converter's capacitor voltage V_c and inductor current i_L are transmitted to the sliding mode controller (SMC), whose output controls the IGBT converter's gate signals. The output of the DC–DC converter is then linked to a space-vector pulse-width-modulated high-power inverter based on voltage-oriented control (VOC), which distributes three-phase power to the micro-grid or isolated three-phase AC loads [9,10].
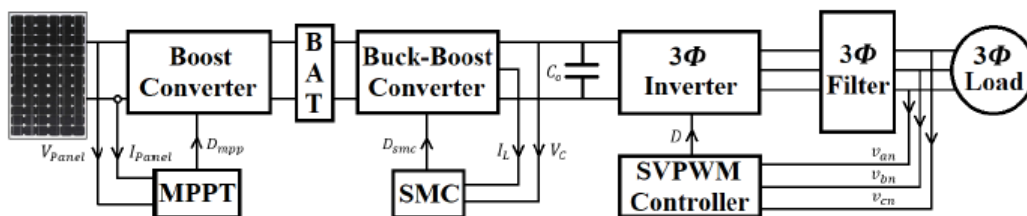
Figure 1: Overall photovoltaic energy conversion system block diagram.

II. Mathematical Modeling of Photovoltaic Modules

Solar irradiance is converted to electrical energy in photovoltaic modules by activating electrons in semiconductor materials such as monocrystalline and polycrystalline silicon. As seen in Figure 2, solar panels are frequently modelled as a single-diode equivalent circuit model.
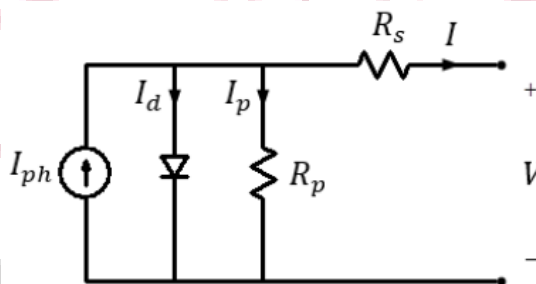

Figure 2: Solar cell single-diode equivalent circuit diagram.

In our research, we used the commercially available "SolarWorld Sunmodule Plus SW 270 Mono Black," whose ratings are detailed in the module data-"Standard sheet's Test Conditions (STC)" section. The STC is carried out under the following conditions:

$$G = 1000 \; \frac{W}{m^2}$$

$$T_{ref} = 25 \; °C$$

$$A.M = 1.5$$

where G, T_{ref} , and A.M denote irradiance (the power of solar radiation perm2), operational cell temperature, and air mass (relative thickness of atmosphere), respectively. The panel's output response under the testing conditions [11] are summarized in Table I.

Table I: SolarWorld Sunmodule Plus SW 270 Mono Black Panel ratings.

P_{max}	270 W_p	Panel rated power at MPP
V_{oc}	39.2 V	Panel open-circuit V
V_{mpp}	30.9 V	Panel rated voltage at MPP
I_{sc}	9.44 A	Panel short-circuit I
I_{mpp}	8.81 A	Panel rated current at MPP
η_m	16.10 %	Panel efficiency
TCP_{mpp}	-0.43 % / °C	Power temperature coefficient at MPP
TCI_{sc}	0.044% / °C	SC temperature coefficient at MPP
TCV_{oc}	-0.31% / °C	OC temperature coefficient at MPP
N_{cell}	60	Number of cells per panel
TYP	Monocrystalline	Cell type

Leveraging KCL in Figure 2, the analytical model for panel output current I becomes

$$I = I_{ph} - I_d - I_p \tag{1}$$

where $I_{ph}, I_d,\ I_p,\ I,\ R_p,\ R_s$ and V denote the current produced by photons, diode current, cell's internal parallel resistance current, cell output current, internal shunt resistance, internal series resistance, and output voltage, respectively. Current produced by photon is represented with a constant current source. It should be noted that photon current I_{ph} depends on solar irradiation and PV cell temperature. The amount of I_{ph} produced by a solar cell is given as

$$I_{ph} = I_{sc} + TCI_{sc}(T_{panel} - T_{ref})(\tfrac{G}{G_{nom}}) \tag{2}$$

Considering semiconductor material properties, diode current I_d becomes

$$I_d = I_{sat}\left[e^{\frac{q(V+(IR_S))}{N_S kA T_{ref}}} - 1\right] \tag{3}$$

Saturation current depends on the reverse-saturation effect of the semiconductor, which can be characterized by (4) and (5).

$$I_{sat} = I_{rev\_sat}\left(\frac{T_{panel}}{T_{ref}}\right)^3\left[e^{\frac{qV_q}{kA}\left(\frac{1}{T_{ref}} - \frac{1}{T_{panel}}\right)}\right] \tag{4}$$

$$I_{rev\_sat} = \frac{I_{SC}}{\left(e^{\frac{qV_{OC}}{N_S kA T_{ref}}}\right) - 1} \tag{5}$$

The internal resistances R_p and R_s can be estimated by using (6) and (7).

$$R_p \approx \frac{100\,V_{OC}}{I_{SC}} \tag{6}$$

$$R_s \approx \frac{0.01\,V_{OC}}{I_{SC}} \tag{7}$$

Hence, the resultant PV panel output current I is finally reached as

$$I = I_{ph} - I_{sat}\left[e^{\frac{q(V+(IR_S))}{N_S kA T_{ref}}} - 1\right] - \frac{V + IR_S}{R_p} \tag{8}$$

where $q, V_q, N_s, k, A, I_{sat}, I_{rev\_sat}$ and G_{nom} are electron charge, crystal-silicon bandgap voltage, number of solar cells in series, Boltzmann's constant, diode ideality factor, diode saturation current, diode reverse-saturation current, nominal solar irradiance, respectively, [12,13].

It should be noted that the PV panel power rating changes as the power temperature coefficient changes, under different panel temperatures. Equation (9) below clarifies how the output power varies, as the ambient temperature changes [1].

$$P_{out} = P_{mpp} + \left[T_{panel} - T_{ref}\right] \times TCP_{mpp} \tag{9}$$

Based on the aforementioned photovoltaic modules ratings, mathematical modelling, and underlying dynamics analysis, single solar panel simulations are conducted in the MATLAB/Simulink environments. The P-V characteristics of the solar panel are shown in Figures 3 and 4, while I-V results are given in Figures 5 and 6 under time-varying solar irradiation and ambient temperature conditions.
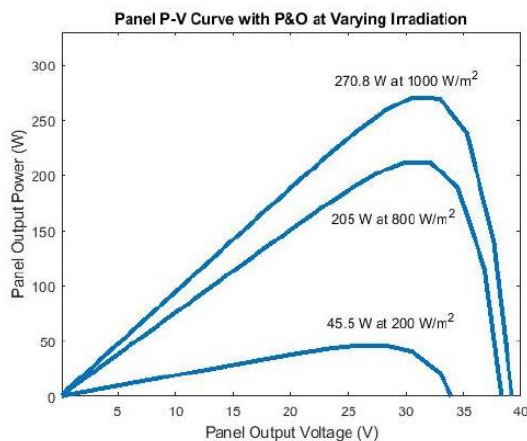

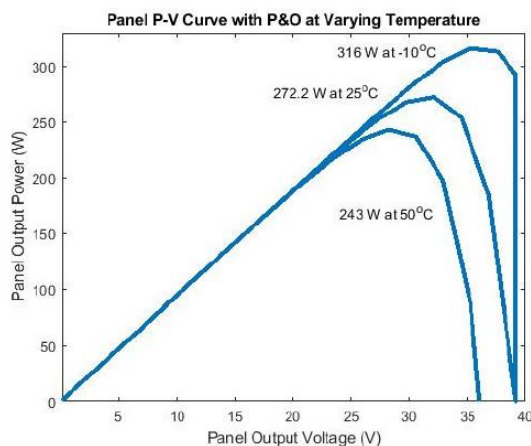Figure 3: P-V characteristic under changing irradiation.

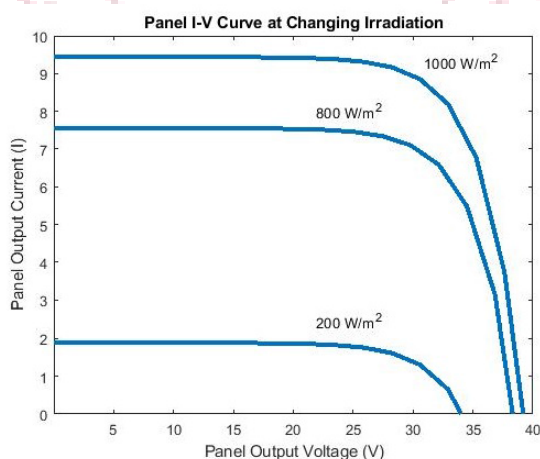Figure 4: P-V characteristic under changing temperature.

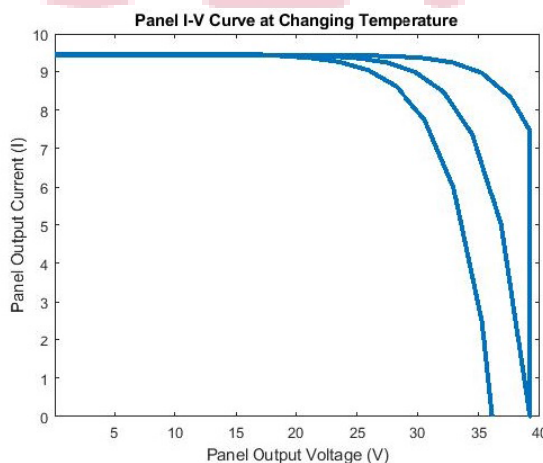Figure 5: I-V characteristic under changing irradiation.

Figure 6: I-V characteristic under changing temperature.

III. Maximum Power Point Tracking Algorithm

Figure 3 shows that when the derivative of each curve, which represents the solar panel output power at different irradiation ratings, is adjusted to zero, P_{mpp} is attained at the maximum power-point. Solar panels would never operate at their maximal power output state if maximum power-point tracking control was not used, and power efficiency would be severely lowered. The perturbation and observation (P&O) (hill climbing) method is an effective and resilient maximum power-point tracking (MPPT) methodology that improves both accuracy and efficiency among many MPPT techniques. The impedance matching qualities of the P&O method allow for optimal power transmission. Because this characteristic is comparable to that of the incremental conductance technique (ICM), the P&O is often referred to as a modified form of ICM [14–25].

The P&O operation starts by sensing panel current I_k and voltage V_k, then the solar panel power can be computed as $P_k = V_k I_k$ and compared with the previous rating P_k - 1 continuously.

$$\Delta P = P_k - P_{k-1} \tag{10}$$
$$\Delta V = V_k - V_{k-1} \tag{11}$$

If the solar panel operating-point is located on the left wing of the maximum powerpoint (MPP), and if power is moving upwards on the graph $\Delta P > 0$, the changes in both power and voltage become positive, i.e., $\Delta P, \Delta V > 0$. In this case, panel voltage is supposed to be increased $\Delta V > 0$ by changing the duty cycle to reach the maximum capable power-rating of the panel. On the other hand, if the panel voltage is increased too much, and the maximum power-point is passed, the PV module voltage needs to be decreased by altering the duty-cycle to reach the peak power-point again $\Delta P. \Delta V < 0$. Moreover, once the maximum power point $\Delta P. \Delta V = 0$ neighborhood is achieved, the duty cycle ripples with a small step size to maintain the operating point, staying within that region. Therefore, the P&O MPPT controller can be self-adjusted to reach the maximum power-point condition.

IV. Nonlinear Dynamics of Buck-Boost Converter

A buck-boost converter topology is shown in Figure 7. The circuit consists of a voltage source (E), inductor (L), capacitor (C), load resistance (R), diode (D), and power switching device (Q). A buck-boost converter has positive polarity on the input voltage and negative polarity on the output voltage.
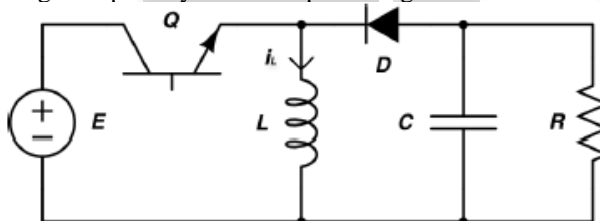

Figure 7: Buck-boost converter diagram.

When the switching device Q is in the conduction mode, current flows through the inductor due to reverse biased diode connection, which energizes the inductor and induces voltage of E. The conduction period is assigned as DT, where D and T are the duty-cycle ratio and the switching period, respectively. When Q is open-circuited, the inductor dis-energizes, and current flows through the resistor via the diode. The voltage across the inductor becomes $-v_{out}$. The non-conducting period is defined as (1 - D)T. The buck-boost converter's equivalent circuit diagrams during the "conducting" and "non-conducting" stages are depicted in Figures 8 and 9.
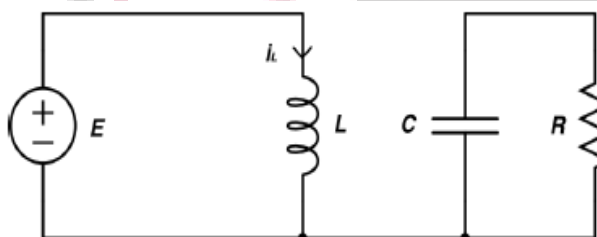

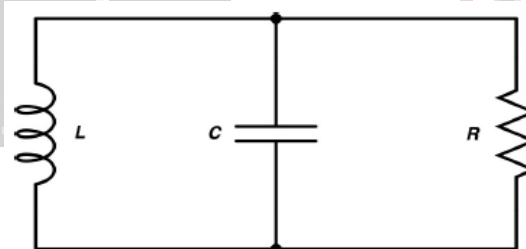Figure 8: Buck-boost converter—switch "ON".

Figure 9: Buck-boost converter—switch "OFF".

Denote u as the system control input. In another word, the switch Q is on when $u - 1$, and is off when $u = 0$. When the switching device is closed-circuited, i.e., $u = 1$, the state-space model of a buck-boost converter is given as

$$L\frac{di_L}{dt} = E$$

$$C\frac{dv_C}{dt} = \frac{-v_c}{R} \tag{12}$$

Similarly, when the switching device is open-circuited, i.e., $u = 0$, we have

$$L\frac{di_L}{dt} = v_C$$

$$C\frac{dv_C}{dt} = -i_L - \frac{-v_c}{R} \tag{13}$$

Equations (12) and (13) can be combined as

$$\frac{di_L}{dt} = (1-u)\frac{v_c}{L} + \frac{E}{L}u$$

$$\frac{dv_C}{dt} = -\frac{v_c}{RC} - (1-u)\frac{i_L}{C} \tag{14}$$

System dynamics can be formulated in the form of x˙ = Ax(t) + Bu(t).

$$\frac{di_L}{dt} = \frac{v_c}{L} + \frac{E-v_c}{L}u \tag{15}$$

$$\frac{dv_C}{dt} = -\frac{i_L}{C} - \frac{v_c}{RC} + \frac{i_L}{C}u \tag{16}$$

Denote x1 = iL and x2 = vc, the A and B matrices become

$$A = \begin{bmatrix} 0 & \frac{1}{L} \\ -\frac{1}{C} & -\frac{1}{RC} \end{bmatrix} \tag{17}$$

$$B = \begin{bmatrix} \frac{E-x_2}{L} \\ \frac{x_1}{C} \end{bmatrix} \tag{18}$$

V. Sliding Mode Control for Buck-Boost Converter

Sliding mode control is a variable structure control approach that applies a discontinuous control input to the nonlinear system dynamics and compels the state trajectories to remain along the sliding boundaries. Due of the quick switching between continuous structures, the sliding mode approach is insensitive to uncertainties. The sliding mode describes the motion of a nonlinear system sliding along these limits. The sliding manifolds are geometrical loci that consist of specified bounds [2,4,7].

Consider the nonlinear system dynamics

$$\dot{x}(t) = g\big(x(t)\big) + \Phi\big(x(t)\big)\cdot u(t) \tag{19}$$

where x(t) is the state variable, g(.) and F(.) are vector fields in the same space. u(t) is the discontinuous control input defined as

$$u(t) = \begin{cases} \cup^+, for\ S(x,t) < 0 \\ \cup^-, for\ S(\&x,t) < 0 \end{cases} \tag{20}$$

(x, t) is the predetermined trajectory where state variable x is driven to track the sliding manifold. U+ and U- are either scalar values or function of x(t). Sliding mode properties can be achieved when the reachability, existence, and Lyapunov stability conditions are satisfied.

The reachability condition makes sure that the sliding manifold will be detected and reached, which can be expressed as

$$S(x)\dot{S}(x) < 0 \tag{21}$$

The existence condition ensures the state trajectory will always be forced to move toward the sliding manifold, once the trajectory is located in the vicinity of the sliding manifold. Existence condition can be analytically represented as

$$\lim_{S \to 0} S(x)\dot{S}(x) < 0 \tag{22}$$

VI. Computer Simulation Studies

According to computer simulations, the solar panels can generate approximately 100 kW of electricity. Figure 10 illustrates the total design schematic. Table 1 shows that 374 panels can generate 100 kW of electricity (17 solar panels in series and 22 panels in parallel). This combination applies to a P&O MPPT-controlled boost converter (17×30.9 V = 525.3 V_{mpp}). By multiplying V_{mpp}, I_{mpp}, and the number of solar panels, the array's precise maximum installed solar power capacity may be computed. As a result, the total electrical power installed is 101.8 kW. Solar irradiation is thought to fluctuate between 600 W/m^2 and 1000 W/m^2, as seen in Figure 11.
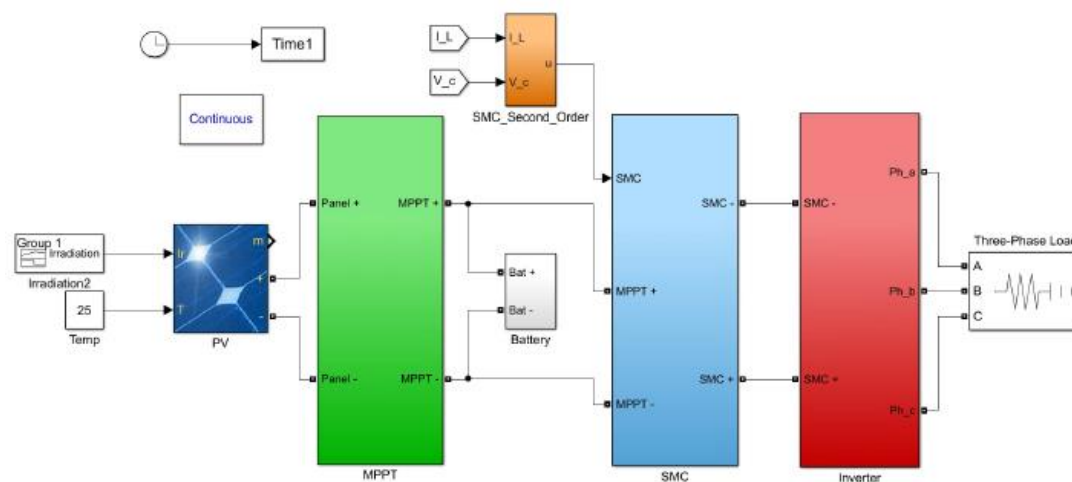
Figure 10: Overall Design.

Photovoltaic panels' output is coupled to an MPPC-controlled boost converter to charge a typical 650 V battery, maximising the solar panels' power generating potential. We propose a first-order and second-order sliding mode controlled (SMC) buck-boost converter to step up voltage from 650 V battery voltage to 1000 V common DC link voltage in order to meet the common DC link voltage of 1000 V. Table 2 summarises the DC–DC power conversion parameters. By stepping up or down the battery voltage, the SMC controlled buck-boost converter gives us the flexibility to meet any common DC link voltage. Furthermore, the voltage-oriented control (VOC) space-vector pulse-width-modulated inverter may directly provide the micro-grid or AC load with three-phase output voltages. A three-phase load was directly supplied by the inverter for computer simulation experiments.

Table II: DC–DC power converter parameters.

-	MPPT Based Boost Converter	SMC Based Buck-Boost Converter
Inductance	33 mH	400 mH
Capacitance	10 mF	1 mF
Input voltage	523.3 V	651 V
Output voltage	651 V	1000 V

Computer simulation results are summarized in the following figures. Figure 11 shows the time-varying solar irradiation in the range between 600 W/m2 and 1000 W/m2 over 10 h daylight duration. Figure 12 illustrates the photovoltaic array output voltage over the changing solar irradiation in Figure 11. Note that the generated voltage from solar panel is about 525 V.
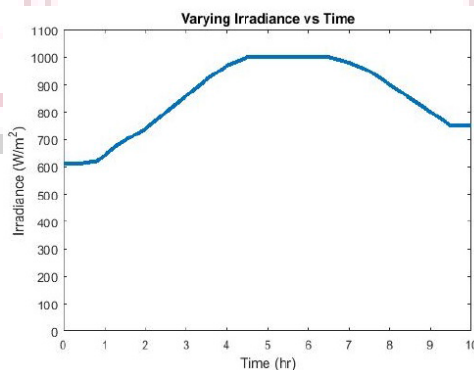

Figure 11: Varying solar irradiation.

Figures 12–14 show that maximum power point of the solar array is accurately tracked by the MPPT controller at 1000 W/m2 irradiation. Figures 15–17 show the P&O based MPPT response under changing irradiation from $600\ W/m^2$ to $1000\ W/m^2$. Hence, the P&O-based maximum powerpoint tracking control successfully ensures high accuracy near the maximum powerpoint ratings ($525.3\ V\ of\ V_{mpp}, 193.8\ A\ of\ I_{mpp}, and\ 101.8\ kW\ of\ P_{mpp}$).
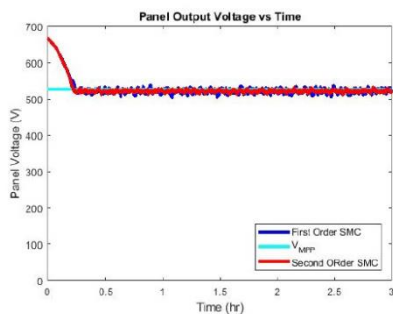
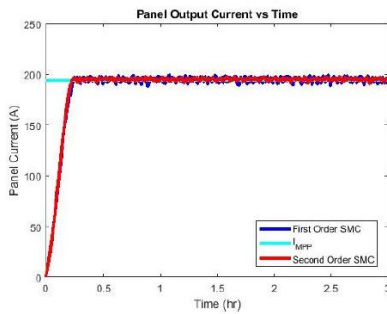Figure 12: PV array output voltage at $1000\ W/m^2$.

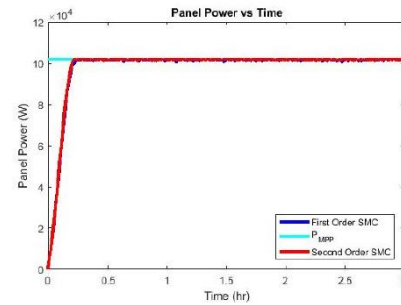Figure 13: PV array output current at $1000\ W/m^2$.

Figure 14: PV array output power at $1000\ W/m^2$

VII. Conclusions

For solar energy conversion systems, new first- and second-order sliding mode controllers (SMC) have been developed. The perturbation and observation (P&O)-based maximum powerpoint tracking (MPPT) approach, which increases the power production efficiency of solar panels amid irradiance changes, may be used to precisely monitor the ideal power-point of solar panels. The SMC-based buck-boost converter can match the battery voltage to the common DC link voltage by stepping up and down the voltage. The voltage-oriented control (VOC)-based space vector pulse-width-modulated inverter uses the common DC connection to deliver three-phase power to the micro-grid or industrial AC loads.

References

[1]   Dunlop, J.P. Photovoltaic Systems, 2nd ed.; American Technical Publishers: Orlando Park, IL, USA, 2010.

[2]   Sira-Ramirez, H.; Rios-Bolivar, M. Sliding mode control of DC-to-DC power converters via extended linearization. IEEE Trans. Circuits Syst. Fundam. Theory Appl. **1994**, 41, 652–661.

[3]   Tan, S.-C.; Lai, Y.M.; Tse, C.K. A unified approach to the design of PWM-based sliding-mode voltage controllers for basic DC–DC converters in continuous conduction mode. IEEE Trans. Circuits Syst. Regul. Pap. **2006**, 53, 1816–1827.

[4]   Reitz, M.A.;Wang, X. Robust sliding mode control of buck-boost DC–DC converters. In Proceedings of the ASME 2016 Conference on Dynamic Systems and Control (DSCC 2016-9804), Minneapolis, MN, USA, 12–14 October 2016; pp. 1–10.

[5]   Oucheriah, S.; Guo, L. PWM-based adaptive sliding-mode control for boost DC–DC converters. IEEE Trans. Ind. Electron. **2013**, 60, 3291–3294.

[6]   P. Mahapatra and C. Gupta, "Study of Optimization in Economical Parameters for Hybrid Renewable Energy System," Res. J. Eng. Technol. …, no. 2581, pp. 39–46, 2020, [Online]. Available: http://www.rjetm.in/RJETM/Vol03_Issue02/Study of Optimization in Economical Parameters for Hybrid Renewable Energy System.pdf.

[7]   A. Hridaya and C. Gupta, "Hybrid Optimization Technique Used for Economic Operation of Microgrid System," Academia.Edu, vol. 5, no. 5, pp. 5–10, 2015, [Online]. Available: http://www.academia.edu/download/43298136/Aditya_pape_1.pdf.

[8]   D. Kumar and C. Gupta, "Multilevel Current-Source Inverter Grid-Connected Analytical Control Approach III . Comparative Performance Evaluation of the CSI Based PV System with the VSI Based PV," Res. J. Eng. Technol. Med. Sci., vol. 2, no. 2, pp. 51–54, 2020.

[9]   A Hridaya; C Gupta, "AN OPTIMIZATION TECHNIQUE USED FOR ANALYSIS OF A HYBRID SYSTEM ECONOMICS," Int. J. Curr. Trends Eng. Technol., vol. 1, no. 6, pp. 136–143, 2015, [Online].

[10]   K. Jagwani, "Contemporary Technological Solutions towards fulfilment of Social Needs A Design Analysis of Energy Saving Through Regenerative Braking in Diesel Locomotive with Super-capacitors," pp. 94–99, 2018.

        Perruquetti,W.; Barbot, J.P. (Eds.) Sliding Mode Control in Engineering; Marcel Dekker: New York, NY, USA, 2002.

[11]   Liu, J. Sliding Mode Control Using MATLAB; Academic Press: Cambridge, MA, USA, 2017.

[12]   Ling, R.; Maksimovic, D.; Leyva, R. Second-Order Sliding-Mode Controlled Synchronous Buck DC–DC Converter. IEEE Trans. Power Electron. **2016**, 31, 2539–2549.

[13]   Wu, B.; Lang, Y.; Zargari, N.; Kouro, S. Power Converters in Wind Energy Conversion Systems; Wiley-IEEE Press: Hoboken, NJ, USA, 2011; pp. 87–152.

[14]   Khanna, R.; Zhang, Q.; Stanchina,W.E.; Reed, G.F.; Mao, Z. Maximum Power Point Tracking Using Model Reference Adaptive Control. IEEE Trans. Power Electron. **2014**, 29, 1490–1499.

[15]   Khanna, R.; Zhang, Q.; Stanchina,W.E.; Reed, G.F.; Mao, Z. Maximum Power Point Tracking Using Model Reference Adaptive Control. IEEE Trans. Power Electron. **2014**, 29, 1490–1499.

[16]   Sunmodule Plus SW 270 Mono Black, User Manual, SolarWorld. Available online: www.solarworld.com (accessed on 10 August 2021).

[17]   de Brito, M.A.G.; Galotto, L.; Sampaio, L.P.; Melo, G.D.A.E.; Canesin, C.A. Evaluation of the Main MPPT Techniques for Photovoltaic Applications. IEEE Trans. Ind. Electron. **2013**, 60, 1156–1167.

[18]   Babu, B.C.; Gurjar, S. A Novel Simplified Two-Diode Model of Photovoltaic (PV) Module. IEEE J. Photovolt. **2014**, 4, 1156–1161.

[19]   Femia, N.; Petrone, G.; Spagnuolo, G.; Vitelli, M. Power Electronics and Control Techniques for Maximum Energy Harvesting in Photovoltaic Systems; CRC Press: Boca Raton, FL, USA, 2013.

[20]   Reitz, M.A. Nonlinear Robust Control of Permanent Magnet Synchronous Motors with Applications to Hybrid Electric Vehicles. Master's Thesis, Southern Illinois University, Edwardsville, IL, USA, May 2016.

[21]   Gursoy, M. Sliding Mode Power Electronics Control for Stand-Alone Photo-Voltaic Energy Systems. Master's Thesis, Southern Illinois University, Edwardsville, IL, USA, May 2019.